

*to be submitted to IEEE EDL*

**7 $\mu$ m Cutoff PtSi Schottky Infrared Detector with Low Dark Current Characteristics**

T. L. Lin, J. S. Park, S. D. Gunapala, E. W. Jones, and H. M. Del Castillo

Center for Space Microelectronics Technology

Jet Propulsion Laboratory, California Institute of Technology

Pasadena, CA 91109

M. M. Weeks and P. W. Pellegrini

Rome Laboratory

Hanscom AFB, MA 01731

## ABSTRACT

**PtSi Schottky** infrared (IR) detectors with extended cutoff wavelengths of 5.7, 6.6, and 7.3  $\mu\text{m}$  have been demonstrated by incorporating thin  $\text{p}^+$  layers with various thicknesses at the **PtSi/Si** interface. Contrary to the 20-50 meV discrepancies between the optical potential barrier ( $\Psi_0$ ) and the thermal potential barrier ( $\Psi_t$ ) observed in the conventional **PtSi** detectors, our **PtSi** detectors fabricated by a co-evaporation technique show smaller discrepancies between  $\Psi_0$  and  $\Psi_t$ . These small discrepancies result in a significantly reduced detector dark current.

## 1. INTRODUCTION

**PtSi** Schottky infrared (IR) detectors offer promise of a low-cost, rugged, medium wavelength infrared (MWIR) thermal imaging technology [1]. **PtSi** technology has advantages in silicon-based fabrication, producibility, array size, response uniformity, and low 1/f noise [2-6]. 640 x 480 and 1024 x 1024 element **PtSi** imaging arrays have been demonstrated and are commercially available [2-5]. The low 1/f noise and the good uniformity of the **PtSi** arrays allow precise calibration of array response for spatial non-uniformity compensation, achieving a 0.1 K NEDT at f/1.2 [5].

The spectral response of the **PtSi** Schottky IR detector follows the modified Fowler equation, given by

$$\eta = C_1 \frac{(h\nu - \Psi_0)^2}{h\nu} = 1.24 C_1 \lambda \left( \frac{1}{\lambda} - \frac{1}{\lambda_c} \right)^2 \quad (1)$$

where  $\eta$  is the quantum efficiency (QE),  $C_1$  is the emission coefficient,  $h\nu$  and  $\lambda$  are the energy and the wavelength of the incident photon, respectively, ' $\Psi_0$ ' is the optical potential barrier, and  $\lambda_c$  is the cutoff wavelength, given by

$$\lambda_c = \frac{1.24}{\Psi_0} \quad (2)$$

The cutoff wavelengths  $\lambda_c$  of conventional **PtSi** detectors range from 5.1 to 5.9  $\mu\text{m}$  [7] and consequently, the QE of the **PtSi** detector in the MWIR regime is relatively low as indicated by Eq. 1. The low response of the **PtSi** detector limits its use for night imaging at ambient temperature above freezing. Below freezing, most **PtSi** cameras lose image contrast as the sensor system noise becomes dominant [8].

Furthermore, imagers working in the 4.4 to 5.0  $\mu\text{m}$  spectral region provide similar day and night target signatures which will dramatically reduce the imaging system complexity, because the solar reflection signals of daytime thermal imaging can be greatly suppressed [8]. Therefore, the extension of the **PtSi** cutoff wavelength to 7  $\mu\text{m}$  will increase the detector response, not only giving significant improvement in the cold

night imaging performance but also allowing the effective use of the 4.4 to 5.0  $\mu\text{m}$  spectral band.

Previously, we have demonstrated that by incorporating a 1-rim-thick  $p^+$  doping spike at the PtSi/silicon interface, the PtSi cutoff wavelength can be extended to 22  $\mu\text{m}$  [9]. This doping-spike technique takes advantages of the strong Schottky image force within  $\sim 1$  nm from the PtSi/Si interface [10]. The barrier reduction  $\Delta\psi$  is given approximately by

$$\Delta\psi = \frac{q}{2\epsilon_s} N d^2, \quad (3)$$

where  $N$  and  $d$  are the doping concentration and the thickness of the doping spike, respectively. Therefore, the effective potential barrier can be reduced by adjusting either the doping concentration or the thickness of the doping spikes. Cutoff wavelengths of 14, 18, and 22  $\mu\text{m}$  have been previously demonstrated with thermionic emission limited I-V characteristics and Fowler-dependent photoresponses by increasing the doping concentration of the 1-rim-thick doping spike [9].

It has been reported that for the PtSi detector, the thermal potential barrier  $\psi_t$  is usually 20-50 meV lower than the optical potential barrier  $\psi_o$  [8]. The thermal potential barrier  $\psi_t$  can be determined by the Richardson's plot, i.e.,

$$\ln\left(\frac{J_0}{T^2}\right) = -\frac{\psi_t}{kT} + \ln(A^{**}), \quad (4)$$

where  $J_0$  is the dark current density,  $T$  is the absolute temperature, and  $A^{**}$  is the Richardson constant. This discrepancy results from the fact that the photo-excited carriers suffer inelastic lattice scattering prior to the carrier emission. Therefore, a lower operating temperature is required for the PtSi detectors compared to detectors without the potential barrier discrepancy. This cooling penalty worsens as the cutoff wavelength increases and the potential discrepancy becomes comparable to the reduced potential barrier.

. In this paper, we demonstrated that by varying the spike thickness from 0.7 to 1.1 nm, cutoff wavelengths ranging from 5.7 to 7.3  $\mu\text{m}$  can be obtained using the doping-spike technique. Furthermore, by utilizing a new PtSi formation technique, which involves co-evaporating Pt and Si in a 1:1 ratio onto Si substrates heated at 450°C, the optical potential barriers  $\Psi_o$  (determined by the modified Fowler plots) were found in close agreement (difference  $\approx 10$  meV) with their thermal potential barriers  $\Psi_t$  (determined by the Richardson plots), resulting in a significant improvement in the detector dark current characteristics.

## II. DETECTOR FABRICATION

Three doping-spike PtSi detectors with spike thicknesses of 0.7 nm (sample A), 0.9 nm (sample B), and 1.1 nm (sample C) were fabricated on double-side polished Si (100) wafers with a resistivity of 30  $\Omega\text{-cm}$ . The boron doping concentration of these spikes was  $\sim 5 \times 10^{19} \text{ cm}^{-3}$ . The details of the MBE growth of the p+ doping spikes were given elsewhere [9]. The 4-nm-thick PtSi layers were formed *in-situ* by co-evaporating Pt and Si in a 1:1 ratio onto the Si substrates heated at 450°C. The device structure incorporated n-type guard rings which define the periphery of the active device areas to suppress the edge leakage. Neither an anti-reflection coating nor an optical cavity was incorporated in these test devices.

## III. DETECTOR CHARACTERISTICS

Figure 1 shows the typical dark current characteristics of the PtSi detector with a 1.1-nm-thick doping spike (sample C) at temperatures ranging from 80 to 140K. The active device area is  $4 \times 10^{-4} \text{ cm}^2$ . Thermionic-emission limited current characteristics were clearly observed, indicating the absence of tunneling effects. The Richardson plots of the three doping-spike PtSi detector samples at -0.5 V bias are shown in Fig. 2. Thermal potential barriers  $\Psi_t$  of 0.218, 0.193, and 0.166 eV were determined by Eq. 4

for sample A, B, and C, respectively. As expected from Eq. 3, the potential barrier decreased with increasing spike thickness.

The spectral response was measured with back-side illumination using a blackbody source. The detectors were cooled to 40K and biased at -0.5 V. Figure 3 shows the external QE of sample C as a function of the wavelength. The detector was responsive at wavelengths beyond the 5.5  $\mu\text{m}$  cutoff of the conventional PtSi detector, The cutoff wavelength of sample C was determined to be 7.3  $\mu\text{m}$  by the modified Fowler plot. The plots of  $\sqrt{\eta} h\nu$  versus  $h\nu$  for these detectors are shown in Fig. 4, Optical potential barriers  $\Psi_o$  of 0.217, 0.189, and 0.170 eV were determined from the linear portions of the plots, corresponding to cutoff wavelengths of 5.7, 6.6, and 7.3  $\mu\text{m}$  for sample A, B, and C, respectively. The differences between the optical and the thermal barriers were small for these doping-spike PtSi detectors, suggesting that the photo-excited carriers suffered less inelastic scattering in these PtSi layers. The thermal potential barriers  $\Psi_t$ , the Richardson constants  $A^{**}$ , the optical potential barriers  $\Psi_o$ , the cutoff wavelength  $\lambda_c$ , and the emission coefficient  $C_1$  for these doping-spike PtSi detectors are shown in Table I.

#### IV. SUMMARY

PtSiIR detectors with cutoff wavelengths extended beyond 7  $\mu\text{m}$  were demonstrated. The cutoff wavelengths were shown to increase with increasing doping-spike thickness. Small discrepancies were observed between the thermal and the optical potential barriers for these PtSi detectors fabricated by co-evaporating Pt and Si in a 1:1 ratio onto heated Si substrates.

#### ACKNOWLEDGMENTS

The work described in this report was performed by the Center for Space Microelectronics Technology, Jet Propulsion Laboratory, California Institute of Technology and was jointly sponsored by the National Aeronautics and Space Administration/Office of Advanced Concepts and Technology, and the Ballistic Missile Defense Organization/Innovative Science and Technology Office.

## REFERENCES

- [1] F. D. Shepherd, "Silicide infrared staring sensors," *Proc. SPIE*, vol. 930, p.1, 1988.
- [2] D. J. Sauer, F. V. Shallcross, F. L. Hsueh, G. M. Meray, P. A. Levine, H. R. Gilmartin, T. S. Villani, B. J. Esposito, and J. R. Tower, "640 x 480 MOS PtSi IR sensors," *Proc. SPIE*, Vol. 1540, *Infrared Technology XVII*, edited by B. F. Andresen, M. Scholl, and I. J. Spiro, pp. 285-296 (SPIE, Bellingham, 1991).
- [3] J. L. Gates, W. G. Connelly, T. D. Franklin, R. E. Mills, F. W. Price, and T. Y. Wittwer, "488 x 640-element platinum silicide Schottky focal plane array," *Proc. SPIE*, Vol. 1540, *Infrared Technology XVII*, edited by B. F. Andresen, M. Scholl, and I. J. Spiro, pp. 297-302, (SPIE, Bellingham, 1991).
- [4] D. L. Clark, J. R. Berry, G. L. Compagna, M. A. Cosgrove, G. G. Furman, J. R. Heydweiller, H. Honickman, R. A. Rehberg, P. H. Solie, and E. T. Nelson, "Design and performance of a 486 x 640 pixel platinum silicide IR imaging system," *Proc. SPIE*, Vol. 1540, *Infrared Technology XVII*, edited by B. F. Andresen, M. Scholl, and I. J. Spiro, pp. 303-311, (SPIE, Bellingham, 1991).
- [5] M. Kimata, N. Yutani, and S. N. Tsubouchi, "High performance 1040 x 1040 element PtSi Schottky-barrier image sensor," *Proc. SPIE*, Vol. 1762, *Infrared Technology XVIII*, edited by B. F. Andresen and F. D. Shepherd (SPIE, Bellingham, 1992)
- [6] J. M. Mooney, "Excess low-frequency noise in PtSi on p-type Si Schottky diodes," *IEEE Trans. Electron Devices*, vol. ED-38, p. 160, 1991.
- [7] F. D. Shepherd, "Infrared internal emission detectors," *SPIE Proceedings*, Vol. 1735, *Infrared Detectors: State of the Art*, edited by W. H. Makky, pp. 250-261, 1992.
- [8] F. D. Shepherd, "B-52 IR camera advanced technology transition demonstration," Meeting of the IRIS Specialty Group on Passive Sensors, Ed. M. Cantella, IRIS-IRIS Report NO. 213400-131-X(I), vol. 1, pp. 333-345, 1992.

- [9] T. L. Lin, J. S. Park, T. George, E. W. Jones, R. W. Fathauer, and J. Maserjian, "Long-wavelength **PtSi** infrared detectors fabricated by incorporating a  $p^+$  doping spike grown by molecular beam epitaxy," *Appl. Phys. Lett.*, vol. 62, pp. 3318-3320, 1993.
- [10] S. M. Sze, *Physics of Semiconductor Devices* (Wiley, New York, 1981), Chap. 5.

## FIGURE CAPTIONS

- Figure 1. Reverse dark current characteristics of atypical 7.3 $\mu$ m cutoff doping-spike PtSi detector (sample C) at temperatures ranging from 80 to 140 K. The active detector area is  $4 \times 10^{-4} \text{ cm}^2$ .
- Figure 2. Richardson Plots for the doping-spike PtSi detectors biased at -0.5V. The spike thicknesses for sample A, B, and C are 0.7, 0.9, and 1.1 nm, respectively.
- Figure 3. Spectral response of a typical 7.3  $\mu$ m cutoff backside-illuminated doping-spike PtSi detector (sample C). Neither an optical cavity nor an anti-reflection coating was incorporated in this detector.
- Figure 4. Modified Fowler Plots of  $\sqrt{\eta} h\nu$  versus  $h\nu$  for these doping-spike PtSi detectors at a reverse bias of 0.5 V.  $C_1$  and  $\Psi_0$  were determined from the slopes and the intercepts of the linear curve fits.

TABLE 1. The doping-spike thicknesses, the thermal potential barriers  $\Psi_t$ , the Richardson constants  $A^{**}$ , the optical potential barriers  $\Psi_o$ , the cutoff wavelength  $\lambda_c$ , and the emission coefficient  $C_1$  for these doping-spike PtSi detectors.

	spike thickness (rim)	Thermal potential $\Psi_t$ (eV)	$A^{**}$ ( $\text{Acm}^{-2}\text{K}^{-2}$ )	Optical potential $\Psi_o$ (eV)	$C_1$ (A/w)	$\lambda_c$ ( $\mu\text{m}$ )
A	0.7	0.218	46.3	0.217	0.12	5.74
B	0.9	0.193	72,8	0.189	0.23	6.56
C	1.1	0.166	12.0	0.170	0.17	7.30

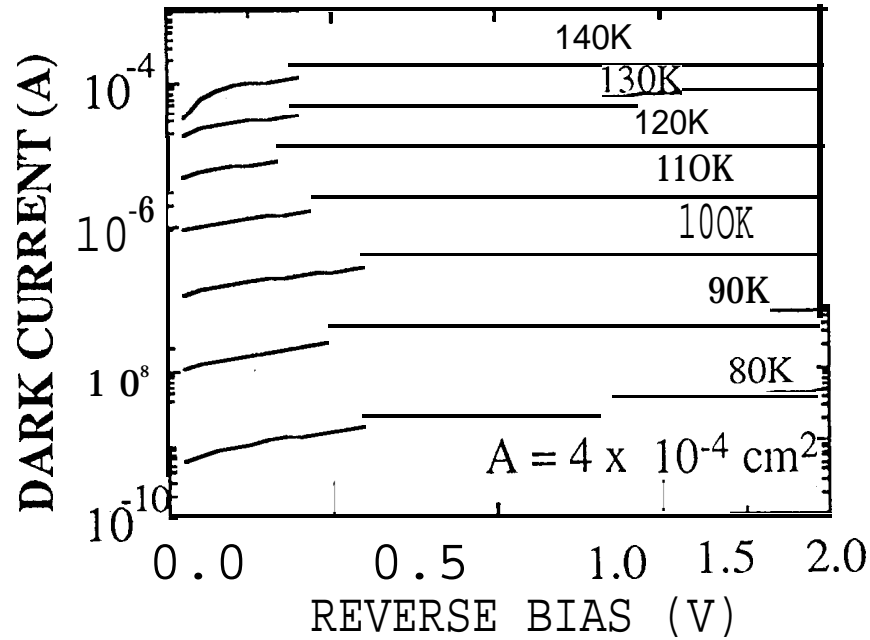


Figure 1. Reverse dark current characteristics of a typical 7.3  $\mu\text{m}$  cutoff doping-spike PtSi detector (sample C) at temperatures ranging from 80 to 140 K. The active detector area is  $4 \times 10^{-4} \text{ cm}^2$ .

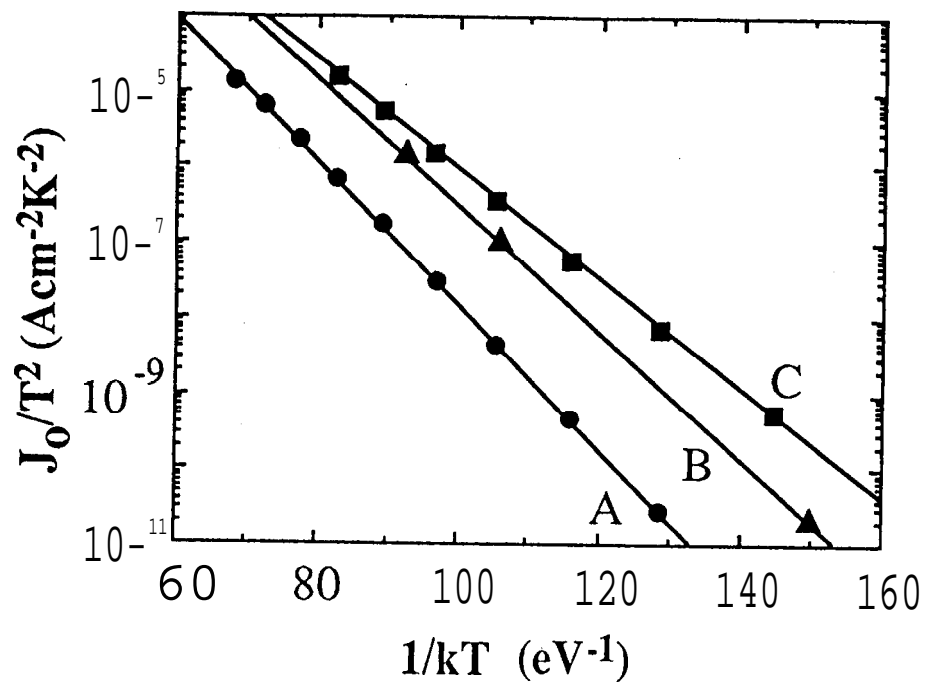


Figure 2. Richardson Plots for the doping-spike PtSi detectors biased at  $-0.5\text{V}$ . The spike thicknesses for sample A, B, and C are 0.7, 0.9, and 1.1 nm, respectively.

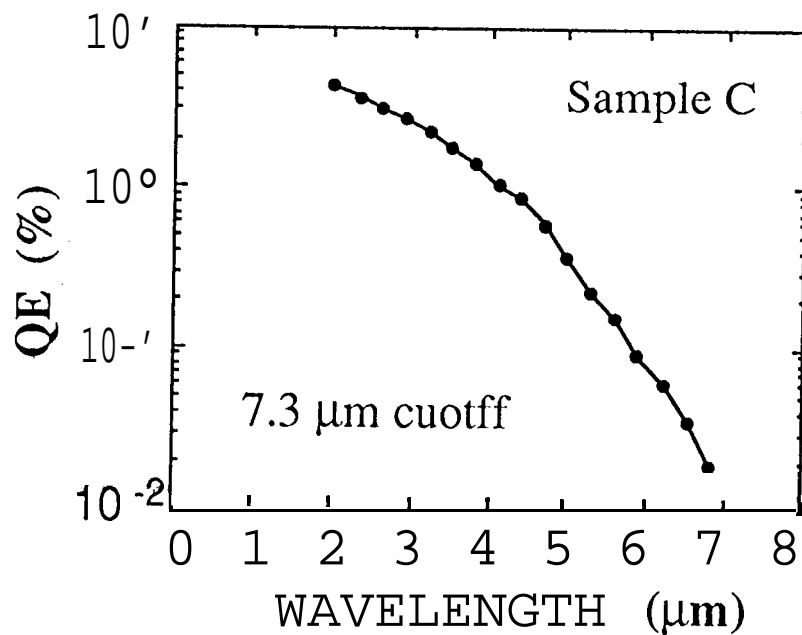


Figure 3. Spectral response of a typical  $7.3\text{ }\mu\text{m}$  cutoff backside-illuminated doping-spike PtSi detector (sample C). Neither an optical cavity nor an anti-reflection coating was incorporated in this detector.

